

Topological superconductivity in EuS/Au/superconductor heterostructures

Ying-Ming Xie,¹ K. T. Law,^{1,*} and Patrick A. Lee^{2,†}

¹*Department of Physics, Hong Kong University of Science and Technology, Clear Water Bay, Hong Kong, China*

²*Department of Physics, Massachusetts Institute of Technology, Cambridge MA 02139, USA*

(Dated: March 19, 2022)

In recent years, signatures of Majorana fermions have been demonstrated experimentally in several superconducting systems. However, finding systems which can be scaled up to accommodate a large number of Majorana fermions for quantum computation remains a major challenge for experimentalists. In a recent work [1], signatures of a pair of Majorana zero modes (MZMs) were found in a new experimental platform formed by EuS islands deposited on top of a gold wire which were made superconducting through proximity coupling to a superconductor. In this work, we provide a theoretical explanation for how MZMs can be formed in EuS/Au/superconductor heterostructures. This simple experimental setup provides a new route for realizing a large number of Majorana fermions for quantum computations.

Introduction.—Recently, there has been intense interest in creating Majorana fermions in condensed matter systems. Of special interest are the Majorana zero modes (MZMs), which have been proposed to be building blocks of fault-tolerant quantum computers [2, 3]. The MZMs have been proposed to exist in the vortex cores of two-dimensional (2D) p -wave superconductors [4] or the ends of 1D p -wave superconductors [5]. Recent efforts have focused on engineering structures where conventional superconductors can induce topological superconductivity via proximity effect [6, 7]. Examples of these candidate topological superconductors include superconductivity proximitized topological insulators [6], semiconductor nanowires [8–13], magnetic atom chains [14–16], and higher order topological insulators [17]. After nearly a decade of intense study, signatures of MZMs have been observed in many condensed matter platforms [17–31]. However, finding an experimental platform which can easily scale up for creating and entangling a large number of Majorana fermions for quantum computation remains a major challenge.

Recently, ferromagnetic EuS islands were deposited on gold wires and zero-bias peaks were observed simultaneously at the two ends of the EuS islands [1]. The observations were taken as evidence for the simultaneous appearance of MZMs at opposite ends of a topological superconductor. The schematic experimental setup is shown in Fig. 1a. This setup is based on the original proposal of Potter and Lee [32], which pointed out that the quasi-one-dimensional gold wires with [111] surface states can be used to realize topological superconductors. The advantage of gold [111] surfaces is that they exhibit strong Rashba spin-orbit coupling (SOC) which causes a band splitting of about 110 meV and the SOC is several orders of magnitude larger than those in semiconductor nanowires [18]. The large Rashba SOC can ensure that the proximity superconducting pairing gap induced on the gold surface state is large even under a strong magnetic field.

However, the original proposal of Potter and Lee [32]

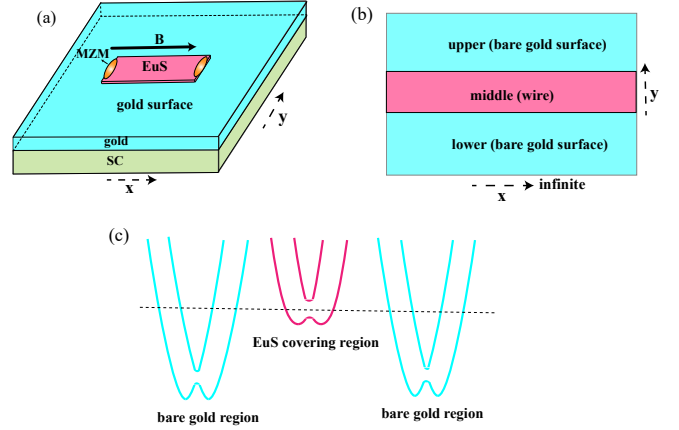


FIG. 1. (a) The schematic figure of EuS/Au/superconductor heterostructure used in ref. [1]. An EuS island is deposited on Au [111] surface which is in proximity to a parent superconductor. Upon applying an in-plane magnetic field \mathbf{B} , MZMs appear at the ends of an EuS island. (b) The geometry employed in our calculation. The upper (U) and lower (L) regions are bare gold surfaces. The middle (M) region is the EuS covered gold surface forming a wire. We take the periodic boundary condition in x -direction so that k_x is a good quantum number and then take the infinite length limit. (c) The schematic picture of the band positions for the bare gold region and the EuS covered region. The dashed line indicates the position of the Fermi energy.

has some limitations. First, the Fermi energy of the gold surface state is relatively high, roughly 500 meV above the band bottom of the surface Rashba band. As a result, many sub-bands will be partially occupied in a quasi-one-dimensional wire at the Fermi energy. For example, roughly 100 sub-bands will be partially occupied if the gold wire is 100 nm wide [1, 32]. This results in a large number of trivial end states co-existing with the MZMs even in the topological regime [32]. Second, the g -factor of gold is about 2 which means that it requires a large external magnetic field to overcome a trivial pairing gap and re-open a topological gap. In the experiment, the

proximity superconducting gap on gold using Vanadium is about 0.5 meV [33]. Therefore, it requires a magnetic field of about 10T to reach the topological regime which is experimentally difficult to achieve. Such a large magnetic field can also severely suppress the superconductivity in the parent superconductor.

Remarkably, it turns out that depositing EuS onto the gold surface solves the two aforementioned limitations at once. First, the surface Rashba band of the gold surface is shifted up so that the Fermi energy is only about 30 meV [1, 33] above the band bottom. At the same time, EuS, being a ferromagnetic insulator, introduces a large exchange field which effectively enhances the Zeeman field [1, 34]. With the EuS/Au/superconductor heterostructure geometry as shown in Fig. 1a, signatures of a pair of MZMs appearing at the opposite ends of an elongated EuS island had been observed using STM measurements when a Zeeman field is applied along the island [1]. In this work, we provide a theoretical account of how Majorana fermions can be generated in EuS/Au/superconductor heterostructures when a EuS island only covers part of the gold surfaces as depicted in Fig. 1a.

Indeed, this is not obvious a priori because the lowering of the chemical potential underneath the EuS means that the potential energy rises underneath the island and repels the electrons from the island rather than confines them. It is true that the gapped superconductor in the gold region outside ultimately confines the quasiparticles under the EuS, but it will be useful to know what role, if any, the potential drop at the edge of the island plays. In this work, we calculate the topological phase diagram of an EuS island deposited on a 2D gold surface which is coupled to a superconductor. We use realistic parameters to describe the spatial inhomogeneity of the electrostatic potential and the inhomogeneous Zeeman field of the heterostructure and evaluate the topological invariant using a modified Green's function method. Our results demonstrate that strips of EuS can be deposited on gold [111] surfaces for the creation of Majorana fermions. Our theory also explains why the localization length of the observed Majorana modes could be much small than the coherence length of the bulk superconductor. The simple fabrication procedures involved in building EuS/Au/superconductor heterostructures provide a new route for creating a large number of Majorana fermions for quantum computation.

Model.— Here, we would like to study the topological properties of a magnetic insulator EuS island deposited on a gold surface which is coupled to a superconductor as depicted in Fig. 1a. We approach this problem by considering a sample shown in Fig. 1b which has periodic boundary conditions in the x -direction so that k_x is a good quantum number, and infinite in the y -direction. The gold surface is separated into three segments, the upper bare gold surface region (U), the lower bare gold

surface region (L) and the EuS covered gold surface in the middle region (M). We compute the topological invariant of this setup taking into account the 2D gold surface. The continuum Hamiltonian that describes this partially covered gold surface state is

$$H = \int dy \sum_{k_x} c_{k_x, \alpha}^\dagger(y) [h_{k_x}^{\alpha\beta}(y) + V(y)\sigma_{\alpha\beta}^x] c_{k_x, \beta}(y), \quad (1)$$

where

$$h_{k_x}(y) = \frac{k_x^2}{2m} - \frac{\partial_y^2}{2m} - \mu(y) + \alpha_R(k_x\sigma^y + i\partial_y\sigma^x). \quad (2)$$

Here, σ^i is the spin operator, α_R is the Rashba velocity characterizing the strength of spin-orbit coupling, $\mu(y)$ and $V(y)$ are the chemical potential and the Zeeman energy respectively.

The y dependence of $\mu(y)$ and $V(y)$ captures the observation [1, 33] that a thin layer of EuS can shift the chemical potential of the surface Rashba band so that the band bottom is moved from 500 meV to around 30 meV compared to the Fermi energy. At the same time, the Zeeman energy is locally enhanced under the ferromagnetic insulator EuS via the exchange coupling, which enables us to drive the gold surface states under the EuS island into the topological region with a relatively small in-plane magnetic field.

We denote μ_0 , V_0 as the chemical potential and Zeeman energy for bare gold surface region where $y \in \{U, L\}$ and μ_{EuS} is the chemical potential for EuS covered gold surface where $y \in M$.

In the numerical calculations where we will integrate out the bare gold regions numerically using lattice green's function method [35–38], we discretize the continuum Hamiltonian H in the y -direction and obtain a lattice Hamiltonian

$$H_0 = \sum_{k_x, j} c_{k_x, j, \alpha}^\dagger ((4t - \mu_j - 2t \cos k_x) \delta_{\alpha\beta} + \alpha_R \sin k_x \sigma_{\alpha\beta}^y + V_j \sigma_{\alpha\beta}^x) c_{k_x, j, \beta} + \sum_{k_x, j} c_{k_x, j, \alpha}^\dagger (-t \delta_{\alpha\beta} + \frac{i}{2} \alpha_R \sigma_{\alpha\beta}^x) c_{k_x, j+1, \beta} + h.c. \quad (3)$$

We set $t = 1/2ma^2 = 16 \text{ eV} \cdot \text{\AA}^2/a^2$, $\alpha_R = 0.4 \text{ eV} \cdot \text{\AA}/a$, which are chosen to recover the realistic continuum band dispersion [39]. The lattice constant a is chosen as 1 nm for the sake of convenience.

In the EuS/Au/superconductor geometry, superconductivity is first induced on the gold bulk states through proximity effect. And the mixing of the gold bulk and surface states via impurity scattering or virtual scattering via phonon or Coulomb interaction can further induce superconductivity onto the surface states. As a result, the proximity effect on the surface states can be described by

a self-energy term [1, 40, 41]

$$\Sigma(\omega^+) \approx -\Gamma \frac{(\omega^+ - V_0 \sigma^x) \tau_0 - \Delta_B \tau_x}{\sqrt{\Delta_B^2 - \omega_+^2}}, \quad (4)$$

where $\omega_+ = \omega + i\eta$, η is an infinitesimal positive number, Δ_B is the superconducting gap of gold bulk states, τ operates on the Nambu particle-hole basis $\Psi(k_x, y) = [c_{k_x, \uparrow}(y), c_{k_x, \downarrow}(y), c_{-k_x, \downarrow}^\dagger(y), -c_{-k_x, \uparrow}^\dagger(y)]^T$, Γ is the gold bulk and surface state mixing strength and is set to be $3\Delta_B$ to explain the experimentally observed superconducting gap on the gold surfaces [1]. More specifically, $\Gamma = \pi N_B(0)W^2$ where $N_B(0)$ is the bulk density of states of gold near Fermi energy and W is the disorder scattering strength which mixes the bulk and the surface states [32]. Therefore, in our formalism, we take into account the effect of the coupling between the bulk states and the surface states of gold and do not use a simple Rashba band to describe the surface state. As we will see below, this indeed has an important effect on the localization length of the Majorana wavefunction of the system [42].

After incorporating the self-energy term, the Green's function of the gold surface state is

$$G_0(\omega, k_x) = \frac{Z}{(\omega^+ - V_x \sigma^x) \tau_0 - Z h_{k_x} \tau_z - (1 - Z) \Delta_B \tau_x}. \quad (5)$$

The quasiparticle weight $Z(\omega_+) = \frac{1}{1 + \Gamma / \sqrt{\Delta_B^2 - \omega_+^2}}$. The effective Zeeman energy V_x is equal to V_0 for the bare gold region, $ZV_{ex} + V_0$ for the surface states under EuS covering region which for simplicity is replaced by its zero frequency limit and denoted as V_{EuS} . Here V_{ex} denotes additional Zeeman energy induced by the ferromagnetic insulator EuS.

Evaluating the Z_2 topological invariant.—The topological class of our model belongs to D class, which in our case is characterized by a Z_2 topological invariant [43]. A simple scheme to obtain this Z_2 topological invariant for a quasi-one-dimensional system is to define a skew-symmetric matrix as $B(k_x) = H(k_x) \tau_y \sigma_y$ based on the particle-hole symmetry operator $\Theta = \tau_y \sigma_y K$, and the Z_2 invariant \mathcal{M} can be obtained as $\text{sgn}[\text{Pf}B(k_x = 0)] \times \text{sgn}[\text{Pf}B(k_x = \pi/a)]$ [9, 44], where Pf denotes the Pfaffian of a matrix. Here $H(k_x)$ is the full Bogoliubov-de Gennes Hamiltonian to model the topological superconductor, K denotes the complex conjugate operator.

However, we cannot directly apply this scheme to evaluate the topological invariant for two reasons. First, we have a frequency-dependence in the self-energy term; second, in order to treat a bare gold surface which is truly 2D, we cannot use $H(k_x)$ directly which describes a quasi-one-dimensional system. The first obstacle can be removed by using the Green's function scheme to evaluate the topological invariant. According to Ref. [45, 46], this scheme can be simplified to obtain the topological invariant from the effective Hamiltonian,

which is expressed in terms of Green's function at zero frequency: $-G^{-1}(\omega = 0, k_x)$. The second obstacle can be overcome by integrating out the two bare gold segments to obtain the self-energy terms $\Sigma_U(\omega, k_x)$ and $\Sigma_L(\omega, k_x)$ which can be added to the Green's function of gold surface covered by EuS. With Dyson's equation, $G(\omega, k_x) = (G_0^{-1}(\omega, k_x) - \Sigma_U(\omega, k_x) - \Sigma_L(\omega, k_x))^{-1}$, the effective Hamiltonian is obtained as

$$h_t(k_x) = h_{k_x}(y \in M) \tau_z + Z(0)^{-1} V_{EuS} \sigma_x + (Z(0)^{-1} - 1) \Delta_B \tau_x + \Sigma_U(0, k_x) + \Sigma_L(0, k_x). \quad (6)$$

$\Sigma_{U(L)}(0, k_x)$ can be calculated from Eq. 5 numerically using the lattice Green's function method [35–38]. The $B(k_x)$ can be defined as $h_t(k_x) \tau_y \sigma_y$, and this new skew-symmetric matrix is used to evaluate the topological invariant \mathcal{M} for our model. One comment is that we take into account the fact that the relatively small Zeeman energy ($\sim 0.2\Delta_B$) in bare gold surfaces cannot close the superconducting gap. This enables the bare gold region to be integrated out without introducing extra singularities into the Green's function.

Phase diagram.—In ref. [1], signatures of a pair of MZMs were observed when a EuS island was placed on a gold wire which was in proximity to a superconductor. Here we show how the EuS/Au/superconductor heterostructure can become a topological superconductor. To model the topological region of a large gold surface case, we consider a heterostructure formed by covering a 60 nm wide EuS strip in the middle of a 2D gold surface. Following the scheme of evaluating Z_2 topological invariant shown in the previous section, the resulting phase diagram is obtained as Fig. 2a. It is interesting to note that the phase diagram in Fig. 2a resembles the phase diagram of superconducting quasi-one-dimensional gold wires subject to a Zeeman field. However, the physical origins of the topological regimes are very different. For quasi-one-dimensional gold wires, the system is topological when superconductivity is induced on a wire with an odd number of sub-bands partially occupied at the Fermi energy. In our current situation, the gold surface is strictly 2D and quasi-one-dimensional sub-bands are not well defined. On the other hand, the Zeeman field induced by the external magnetic field and the EuS can create in-gap Yu-Shiba bands under the EuS island [14, 16]. These in-gap bands are confined to be under the EuS island by the fully gapped gold surface states and the system is described by the effective Hamiltonian in Eq. 6.

This phase diagram is further demonstrated with Fig. 2b,c,d. As the parameter, such as the effective Zeeman energy in this case, is tuned across the phase boundary, the energy gap closes and reopens which signals the topological phase transition. More importantly, as shown in Fig. 2d, there is a sizeable topological gap ($\sim 0.1\Delta_B$)

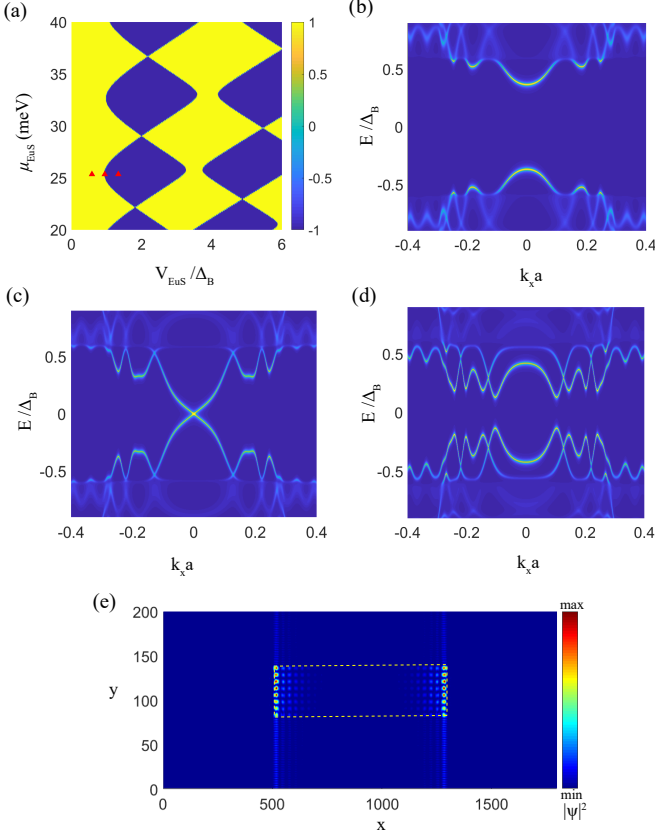


FIG. 2. The topological phase diagram of the heterostructure formed by a 60 nm wide EuS strip and a large gold surface (2D limit here). The width of EuS strip is set to be 60nm. The parameter $\mu_0 = 500$ meV, $V_0 = 0.2\Delta_B$ for bare gold surface are adopted. (a) the topological invariant \mathcal{M} is shown as a function of effective Zeeman energy V_{EuS} and chemical potential μ_{EuS} . The topological trivial region with $\mathcal{M} = 1$ is shown in yellow and topological nontrivial region with $\mathcal{M} = -1$ is shown in blue. (b),(c),(d) show the spectral function $A(k_x, E) = -2\text{Im}(G(\omega, \mathbf{k}_x))$ as a function of k_x and E with the parameters at red triangles shown in (a). The (b),(c),(d) shows the typical exciting feature at the trivial region, phase transition boundary, and topological region respectively. The chemical potential μ_{EuS} of (b),(c), (d) are all chosen to be 25 meV. The V_{EuS} equals $0.5\Delta_B$ for (b), $0.95\Delta_B$ for (c), and $1.5\Delta_B$ for (d). (e) The Majorana wavefunction of a 800 nm \times 60 nm EuS (denoted by the yellow box) deposited on a 2000 nm \times 200 nm Au surface with the parameters of (d). The color indicates the absolute value square of the MZM wavefunction.

deep in the topological region (for example, far away from the topological phase transition boundaries). The Majorana end states using the parameters in Fig. 2d is shown in Fig. 2e. Majorana states residing at the two ends of the EuS island can be clearly observed. It is important to note that these Majorana states are very localized at the ends of the EuS island. However, the localization length of the Majorana mode is much shorter than the bulk superconducting coherence length of gold ξ which is

$\approx t/\Delta_B \approx 320\text{nm}$. This is similar to the case of the short Majorana localization length observed in ferromagnetic atomic chains on Pb substrate [24]. And the short localization length is caused by the normalization effect of the bulk cases which is taken into account through the self-energy term Σ introduced in Eq.5, i.e., t is renormalized as Zt so that the coherence length is renormalized as $Z\xi$. Therefore, our theory also explains the short localization length of the Majorana modes observed in the experiment which is only tens of nm [1].

The effect of the chemical potential step.—In the EuS/Au/superconductor heterostructure with EuS islands deposited on a 2D gold surface, there is a chemical potential step between the area under EuS and the bare gold surface. As shown experimentally, the chemical potential shift indeed depends on the thickness of EuS. When bilayer EuS is deposited on the gold surface, the chemical potential is shifted from $\mu_0 \sim 500$ meV to $\mu_{EuS} \sim 30$ meV relative to the surface Rashba band bottom [1]. On the other hand, if a monolayer EuS is used, the chemical potential is shifted to about 200meV instead [33]. In this section, we study the importance of this chemical potential step. First of all, if we remove this chemical potential step artificially by setting $\mu_0 = \mu_{EuS}$, the phase diagram will change from Fig. 2a into Fig. 3a. Surprisingly, the topological regimes (in blue) become hardly visible, even though the chemical potential is very low. This implies not only the inhomogeneity of Zeeman energy but also the inhomogeneity of chemical potential is important for the observation of a sizeable topological region on a gold surface. It can be seen from Fig. 2a that the separation between the diamond topological regions is roughly 6 meV, which is the same as expected for a wire of the width of the EuS. This suggests the chemical potential step effectively creates a sample width given by EuS width due to the scattering from the potential step.

On the other hand, if EuS with a different thickness or other ferromagnetic insulators are deposited on the gold surface, the shift in chemical potential can be different. In Fig. 3b, we calculated the topological regime with a wide range of chemical potential underneath the ferromagnetic insulator, using the parameters of Fig. 2a except the range of chemical potential used. It is clear from Fig. 3b that a sizeable chemical step between the area covered by the ferromagnetic insulator and the bare gold surface is needed to create large topological regimes.

Conclusion.—Based on the Green's function method, we have evaluated the topological phase diagram of the EuS/Au/superconductor heterostructure. We demonstrated that Majorana fermions can be created when a ferromagnetic island is deposited on a two-dimensional gold surface. The ferromagnetic insulator plays the role of enhancing the Zeeman energy of the gold surface and creates a chemical potential step between the areas covered by the ferromagnet and the bare gold. Our theory

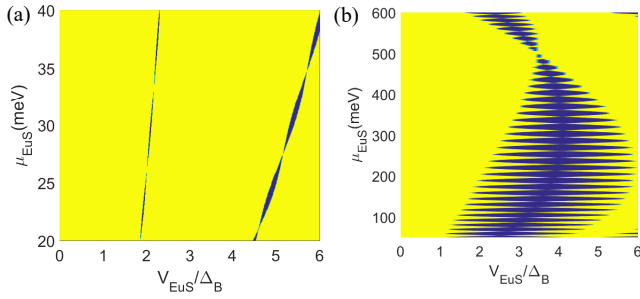


FIG. 3. The effect of chemical potential step between the bare gold surface and the EuS covered region. (a) shows the phase diagram of the heterostructure formed by the EuS strip and the gold surface. The parameters are the same as Fig. 2a, except the chemical potential of the bare gold region artificially set as $\mu_0 = \mu_{EuS}$. The yellow and blue areas represent the topological trivial and nontrivial regimes respectively. (b) The phase diagram as a function of Zeeman energy and the chemical potential of the ferromagnetic insulator covered region. Note the lower range of chemical potential up to 40 meV is given in Fig. 2a. The chemical potential of the bare gold is fixed at $\mu_0 = 500\text{meV}$ for (b).

also explains how the observed Majorana modes can have very short localization length as observed in the recent experiment reported in Ref. [1]. The simple fabrication procedures of the experimental setup discussed would allow experimentalists to create a large number of Majorana modes for quantum computation purposes.

Acknowledgments.— Y.-M. Xie and K. T. Law acknowledges the support of Croucher Foundation, Dr. Tai-chin Lo Foundation and HKRGC through C6026-16W, 16324216, 16307117 and 16309718. PAL acknowledges support by U. S. Department of Energy, Basic energy Science, under grant DE-FG02-03ER46076, John Templeton Foundation Grants No. 39944 and 60148.

* phlaw@ust.hk

† palee@mit.edu

- [1] S. Manna, P. Wei, Y. Xie, K. Tuen Law, P. Lee, and J. Moodera, arXiv:1911.03802. (To appear in Proceedings of National Academy of Sciences).
- [2] A. Kitaev, *Annals of Physics* **303**, 2 (2003).
- [3] C. Nayak, S. H. Simon, A. Stern, M. Freedman, and S. Das Sarma, *Rev. Mod. Phys.* **80**, 1083 (2008).
- [4] N. Read and D. Green, *Phys. Rev. B* **61**, 10267 (2000).
- [5] A. Y. Kitaev, *Physics-Uspekhi* **44**, 131 (2001).
- [6] L. Fu and C. L. Kane, *Phys. Rev. Lett.* **100**, 096407 (2008).
- [7] J. Alicea, *Phys. Rev. B* **81**, 125318 (2010).
- [8] R. M. Lutchyn, J. D. Sau, and S. Das Sarma, *Phys. Rev. Lett.* **105**, 077001 (2010).
- [9] J. D. Sau, R. M. Lutchyn, S. Tewari, and S. Das Sarma, *Phys. Rev. Lett.* **104**, 040502 (2010).
- [10] Y. Oreg, G. Refael, and F. von Oppen, *Phys. Rev. Lett.* **105**, 177002 (2010).
- [11] A. C. Potter and P. A. Lee, *Phys. Rev. Lett.* **105**, 227003 (2010).
- [12] R. M. Lutchyn, T. D. Stanescu, and S. Das Sarma, *Phys. Rev. Lett.* **106**, 127001 (2011).
- [13] Y. Xie, B. T. Zhou, T. K. Ng, and K. T. Law, *Phys. Rev. Research* **2**, 013026 (2020).
- [14] T.-P. Choy, J. M. Edge, A. R. Akhmerov, and C. W. J. Beenakker, *Phys. Rev. B* **84**, 195442 (2011).
- [15] J. Klinovaja, P. Stano, A. Yazdani, and D. Loss, *Phys. Rev. Lett.* **111**, 186805 (2013).
- [16] G. M. Andolina and P. Simon, *Phys. Rev. B* **96**, 235411 (2017).
- [17] B. Jäck, Y. Xie, J. Li, S. Jeon, B. A. Bernevig, and A. Yazdani, *Science* **364**, 1255 (2019).
- [18] V. Mourik, K. Zuo, S. M. Frolov, S. R. Plissard, E. P. A. M. Bakkers, and L. P. Kouwenhoven, *Science* **336**, 1003 (2012).
- [19] L. P. Rokhinson, X. Liu, and J. K. Furdyna, *Nature Physics* **8**, 795 (2012).
- [20] A. Das, Y. Ronen, Y. Most, Y. Oreg, M. Heiblum, and H. Shtrikman, *Nature Physics* **8**, 887 (2012).
- [21] M. T. Deng, C. L. Yu, G. Y. Huang, M. Larsson, P. Caroff, and H. Q. Xu, *Nano Letters* **12**, 6414 (2012).
- [22] S. M. Albrecht, A. P. Higginbotham, M. Madsen, F. Kuemmeth, T. S. Jespersen, J. Nygård, P. Krogstrup, and C. M. Marcus, *Nature* **531**, 206 (2016).
- [23] H. Zhang, C.-X. Liu, S. Gazibegovic, D. Xu, J. A. Logan, G. Wang, N. van Loo, J. D. S. Bommer, M. W. A. de Moor, D. Car, R. L. M. Op het Veld, P. J. van Veldhoven, S. Koelling, M. A. Verheijen, M. Pendharkar, D. J. Pennachio, B. Shojaei, J. S. Lee, C. J. Palmström, E. P. A. M. Bakkers, S. D. Sarma, and L. P. Kouwenhoven, *Nature* **556**, 74 (2018).
- [24] S. Nadj-Perge, I. K. Drozdov, J. Li, H. Chen, S. Jeon, J. Seo, A. H. MacDonald, B. A. Bernevig, and A. Yazdani, *Science* **346**, 602 (2014).
- [25] A. Fornieri, A. M. Whiticar, F. Setiawan, E. Portolés, A. C. C. Drachmann, A. Keselman, S. Gronin, C. Thomas, T. Wang, R. Kallagher, G. C. Gardner, E. Berg, M. J. Manfra, A. Stern, C. M. Marcus, and F. Nichele, *Nature* **569**, 89 (2019).
- [26] H. Ren, F. Pientka, S. Hart, A. T. Pierce, M. Kosowsky, L. Lunczer, R. Schlereth, B. Scharf, E. M. Hankiewicz, L. W. Molenkamp, B. I. Halperin, and A. Yacoby, *Nature* **569**, 93 (2019).
- [27] J.-P. Xu, M.-X. Wang, Z. L. Liu, J.-F. Ge, X. Yang, C. Liu, Z. A. Xu, D. Guan, C. L. Gao, D. Qian, Y. Liu, Q.-H. Wang, F.-C. Zhang, Q.-K. Xue, and J.-F. Jia, *Phys. Rev. Lett.* **114**, 017001 (2015).
- [28] H.-H. Sun, K.-W. Zhang, L.-H. Hu, C. Li, G.-Y. Wang, H.-Y. Ma, Z.-A. Xu, C.-L. Gao, D.-D. Guan, Y.-Y. Li, C. Liu, D. Qian, Y. Zhou, L. Fu, S.-C. Li, F.-C. Zhang, and J.-F. Jia, *Phys. Rev. Lett.* **116**, 257003 (2016).
- [29] D. Wang, L. Kong, P. Fan, H. Chen, S. Zhu, W. Liu, L. Cao, Y. Sun, S. Du, J. Schneeloch, R. Zhong, G. Gu, L. Fu, H. Ding, and H.-J. Gao, *Science* **362**, 333 (2018).
- [30] L. Kong, S. Zhu, M. Papaj, H. Chen, L. Cao, H. Isobe, Y. Xing, W. Liu, D. Wang, P. Fan, Y. Sun, S. Du, J. Schneeloch, R. Zhong, G. Gu, L. Fu, H.-J. Gao, and H. Ding, *Nature Physics*, 1 (2019).
- [31] S. Zhu, L. Kong, L. Cao, H. Chen, M. Papaj, S. Du, Y. Xing, W. Liu, D. Wang, C. Shen, F. Yang, J. Schneeloch, R. Zhong, G. Gu, L. Fu, Y.-Y. Zhang, H. Ding, and H.-J. Gao, *Science* **367**, 189 (2020).

- [32] A. C. Potter and P. A. Lee, *Phys. Rev. B* **85**, 094516 (2012).
- [33] P. Wei, S. Manna, M. Eich, P. Lee, and J. Moodera, *Phys. Rev. Lett.* **122**, 247002 (2019).
- [34] G.-X. Miao and J. S. Moodera, *Physical Chemistry Chemical Physics* **17**, 751 (2015).
- [35] D. S. Fisher and P. A. Lee, *Phys. Rev. B* **23**, 6851 (1981).
- [36] Q. feng Sun and X. C. Xie, *Journal of Physics: Condensed Matter* **21**, 344204 (2009).
- [37] J. Liu, A. C. Potter, K. T. Law, and P. A. Lee, *Phys. Rev. Lett.* **109**, 267002 (2012).
- [38] J. Liu, F.-C. Zhang, and K. T. Law, *Phys. Rev. B* **88**, 064509 (2013).
- [39] S. LaShell, B. A. McDougall, and E. Jensen, *Phys. Rev. Lett.* **77**, 3419 (1996).
- [40] A. C. Potter and P. A. Lee, *Phys. Rev. B* **83**, 184520 (2011).
- [41] J. D. Sau, R. M. Lutchyn, S. Tewari, and S. Das Sarma, *Phys. Rev. B* **82**, 094522 (2010).
- [42] Y. Peng, F. Pientka, L. I. Glazman, and F. von Oppen, *Phys. Rev. Lett.* **114**, 106801 (2015).
- [43] A. P. Schnyder, S. Ryu, A. Furusaki, and A. W. W. Ludwig, *Phys. Rev. B* **78**, 195125 (2008).
- [44] T. D. Stanescu and S. Tewari, *Journal of Physics: Condensed Matter* **25**, 233201 (2013).
- [45] Z. Wang and S.-C. Zhang, *Phys. Rev. X* **2**, 031008 (2012).
- [46] Y. Wang and L. Fu, *Phys. Rev. Lett.* **119**, 187003 (2017).